

ALBA Synchrotron Light Source. Status and perspectives

Inma Peral and Salvador Ferrer

ALBA – CELLS Cerdanyola del Valles, Barcelona (Spain)

Abstract

After a historical introduction of the Alba light source project, a brief description of the main accelerator parameters and of the first seven phase I beamlines currently under construction will be presented. A few examples of applications of diffraction and absorption in samples of geological interest will be presented.

Introduction

At the time Spain joined ESRF as associate member (1987), a few informal meetings were organized by the Research Ministry to discuss on the possibility of having a Synchrotron Source in Spain in the future. This idea was gaining intensity until it materialized somehow in 1994 when the Generalitat of Catalunya already appointed staff to prepare a conceptual design of a source that was presented to authorities in 1998 and that had to wait till 2002 to be approved. The recruitment of the management of the facility started in 2003. From 2004 onwards, a staff of about 140 people was recruited which is distributed in five divisions: Accelerator, Experiments, Computing & Control, Engineering and Administration. Since then, the detailed project of the building and infrastructures, accelerator and beamlines has been continuously progressing. Presently,

(June 2009) the Linac, booster synchrotron and 50 % of the storage ring are installed. Two beamlines have received several optical components which have been installed at the Experimental Hall. According to plans, the first electrons should circulate in the booster by autumn, in the storage ring by Eastern 2010 and the first light to be used for alignment and commissioning purposes shortly after that date. The Laboratory is funded 50-50 by the Ministerio de Investigacion and the Generalitat. It has a Council to which the respective Ministers belong and an Executive Commission

which survey the development of the project. The Director of the project has two consulting bodies: the Machine Advisory Committee and the Scientific Advisor Committee (SAC). The second one had, as first important task, to give recommendations and evaluate the projects of beamlines presented by several groups of users. This process was in fact the end of a trajectory that started in October 2003 in a first meeting of potential users of the future source. Later, in 2004, another meeting was held in Malaga where the projects of the beamlines and the scientists in charge of preparing them were defined. Also, the Spanish organization of users (AUSE) was formally created and since then it has been a very useful communication channel between Alba and the scientific community. In fact, the president of AUSE is formally a permanent invited guest of the SAC. The result of the above process was the selection of seven beamlines to be constructed in first place. Figure 1 shows an aerial view of the laboratory and the inside of the experimental building in September 08.

The Accelerators

Alba is a medium energy third generation synchrotron source similar to the most recent sources build in France (Soleil) or UK (Diamond). This means that the horizontal dimensions of the electron beam and the horizontal divergence are small compared with second generation sources and that the synchrotron radiation is produced mostly with the so called insertion devices which produce intense and very bright photon beams.

The electrons generated by a cold cathode gun are firstly accelerated to 100 MeV by means of a linear accelerator; secondly they are injected into a booster synchrotron which raises the energy up to 3 GeV which is the nominal energy of operation. Then, they are transferred into the circular storage ring of 269 m in length where they are maintained as long as possible. The storage ring has a four fold symmetry. Each quadrant is composed of four cells two of them named matching cells and two regular cells. In the ring there are straight segments where the insertion devices may be installed. These are periodic arrays of magnets which force the electrons to describe curved trajectories which result in the production of intense synchrotron light. These are the main source of synchrotron rad.



Figure 1: a) The Alba synchrotron facility in Sept 2008. b) Aerial view and interior of the Experimental Hall.

They are basically of two types called wigglers and undulators. The insertion devices are designed in accordance with the specific applications of the beamlines that they feed. At the Alba storage ring there are 17 straight sections for insertion devices:

12 of 4 m in length, 3 of 8 meters and 2 of 2.6 meters. All the phase I beamlines except one are feed up with insertion devices installed in 4 m straight sections. More details on the accelerators may be found in Bordas et al. (2004) and Muñoz et al. (2005).

Phase I beamlines

The functionality of the seven beamlines under construction which constitute the Phase I of the beamline portfolio are summarized in the table I.

Beamline	Short name	Photon source	Energy range (keV)	Techniques
High Resol. Powder Diffraction	MSPD	Superconducting wiggler	5-50	Powder diffraction High pressure diff
X ray microscopy	MISTRAL	Bending magnet	0.2 -1	Cryotomography
Non Crystalline Diffraction	NCD	In vacuum undulator	5-15	Small Angle Scattering
Macromolecular Crystallography	XALOC	In vacuum undulator	5-15	Biocrystallography
X ray Absorption Spectroscopy	CLÆS	Wiggler	5-30	Absorption spectroscopy
Spectromicroscopy	CIRCE	Helical Undulator	0.1-1,2	Photoemission microscopy
X ray Magnetic Dichroism	BoReAS	Helical Undulator	0.1-2	Magnetic dichroism, Resonant scattering

Table 1: The functionality of the seven beamlines under construction which constitute the Phase I.

Figure 2 shows the distribution of the beamlines in the Experimental Hall. A brief description of the first group of beamlines follows.

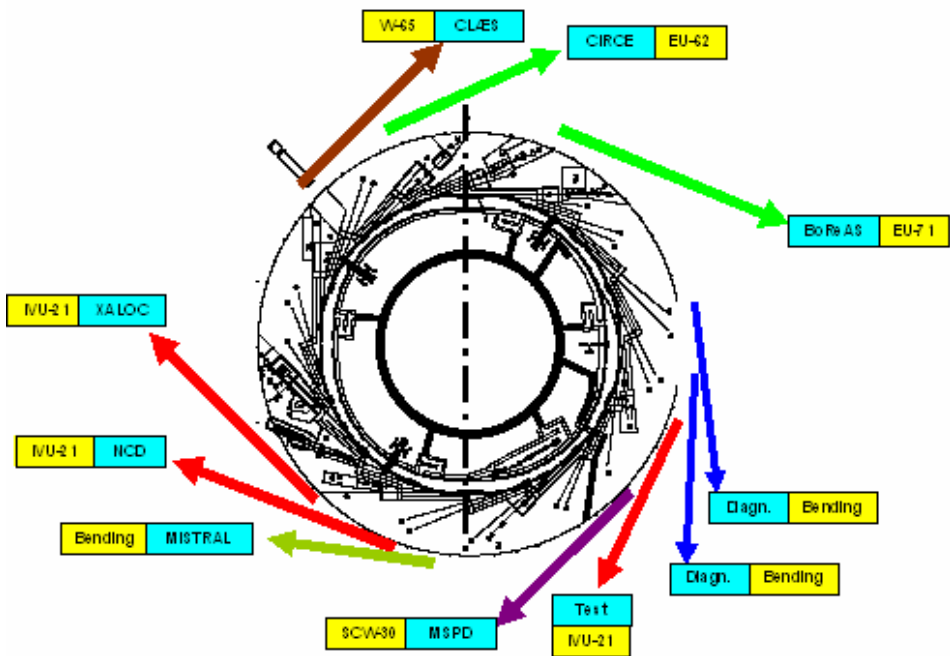


Figure 2. Schematic view of the Experimental Hall and of the locations of the beamlines. The yellow boxes indicate the type of source and the period of the magnetic structure in mm. W-65: wiggler of 65 mm period, EU-62: elliptical undulator of 62 mm period, IVU: in vacuum undulator, SCW: superconducting wiggler. The diagnostic beamlines are for accelerators studies and the test beamline is a development project of an undulator.

- MSPD has a superconducting wiggler as photon source able to generate magnetic fields up to 2T which allow to reach relatively high photon energy. The beamline is installed in port number 4 of the storage ring. The monochromator is a double crystal cryogenically cooled one and the beamline is also equipped with focusing optics mirrors and multilayers. Two end stations will be installed. A three circle θ - 2θ with high angular resolution (0.0002 degrees) diffractometer will accommodate a multichannel (13 Si crystals) analyzer and also a 1D detector for time resolved experiments. Space will be available around the sample position to accommodate small ovens, magnets or other sample environment. A

second instrument located in the experimental hutch will allow to perform high pressure diffraction experiments with diamond anvil cells.

- MISTRAL is a soft X ray beamline (port number 9) specialized in X ray microscopy in the so called water window (above the K edge of C, below the K edge of O). The optics consist in focusing mirrors and in a grating monochromator that delivers photons to a specially designed cryo microscope devoted to tomographic reconstruction of frozen cells. Resolutions around 40 nm will be achieved by means of a Fresnel zone plate objective lens. This microscope is aimed to be complementary to TEM instruments since although the resolution is lower, the samples can be investigated in their integrity, without slicing, due to the high penetration of the x rays relative to the electrons.
- NCD (port 11) is specialized in Small angle Scattering experiments. The source is an in vacuum undulator. The optics consists in a cryogenically cooled Si monochromator followed by a vertically collimated mirror and a toroidal mirror focusing in the detector plane (at 42 meters from the source) with 2:1 demagnification. The end station will be equipped with a large area detector for small scattering angles and with another detector for wide angles the will be possible to operate simultaneously with the first one. A microfocusing optical set up will also be installed for small samples or spatially resolved scattering experiments.
- XALOC (port 13) is devoted to macromolecular crystallography. The source is the same than that of NCD. The optics consists in a double crystal monochromator and a pair of focusing mirrors. The end station has a high precision microdiffractometer, a robot for automatic sample changes and alignments and a 2D detector. The samples will be extracted by the robot from cryogenic containers and will be kept cool during data collection.
- CLÆS (pronounced class) is located in port 22. It is specialized in X ray absorption. The optics consists in a double crystal monochromator and focusing mirrors. In this beamline the monochromator has a special design

that allows to record spectra at relatively fast rates (~ 100 ms) to perform studies of chemical reactions while they are occurring. Chemical reaction cells, specially designed, will allow to monitor the chemical state of the catalysts in *operando* conditions. In addition, the end station will be equipped with an x ray fluorescence analyzer for high resolution spectroscopy or inelastic scattering experiments.

- CIRCE (port 24) is specialized in photoemission experiments. The source is a helical undulator providing elliptical polarization (horizontal, vertical and circular). The beamline has a grating monochromator and mirrors for collimating and focusing. Two end stations devoted to photoemission experiments will be mounted side by side. One of them is a state of the art photoemission microscope (PEEM) with lateral resolution down to 10 nm in the best conditions. Thanks to the variable polarization, magnetic contrast is achievable by means of the magnetic dichroism effect which allows to visualize magnetic domains. The second end station will allow to perform near ambient pressure (20 mbar) photoemission experiments thanks to a differentially pumped set up installed at the entrance of the electron analyzer. This will be particularly useful for surface chemistry studies.
- BoReAS (port 27) is a beamline for XMCD (X ray Magnetic Circular Dichroism) and Resonant Scattering experiments in the soft x ray regime. The source is similar to that of CIRCE and so is the optics. The XMCD station is a 7T cryomagnet and a liquid He sample holder. The main magnetic field is along the photon beam axis and another weaker field (1 T) generated with a different coil will be available in a direction normal to the photon beam. The resonant scattering apparatus will also have a sample manipulator able to operate at liquid He temperatures and a diffractometer.

Some selected examples

Role of synchrotron-based high pressure research

Understanding planetary structure requires a detailed knowledge of the properties of geological materials under conditions of deep planetary interiors. Experiments under such extreme conditions are challenging, however many fundamental properties remain poorly constrained or are inferred only through certain extrapolations from lower pressure-temperature states. The development of dedicated beamlines for high pressure research at both second and third generation synchrotron sources has been a synergistic development which has not only led to advances in analytical capabilities but has also stimulated new developments in pressure and temperature generating apparatus (part III of Hazen and Downs, 2000).

Experimental techniques :Diamond anvil cell

The development of apparatus to maintain materials at high hydrostatic pressures has been an active area of research for many years. The diamond anvil cell has become the standard tool for the generation of high pressures over the last four decades and has been applied in a wide range of experimental studies.



Figure 3: Parts of the Diamond anvil cell (from <http://www.crystal.vt.edu/crystal/dac.html>).

In a diamond anvil cell, a sample is uniaxially compressed between two gem-quality diamonds (see figures 3 and 4). Two advantages of the diamond cell has lead to its widespread use in deep Earth studies: (1) very high pressures up to and beyond 100 GPa; (2) the diamond windows are transparent across wide regions of the electromagnetic spectrum. The former means that, essentially, the entire pressure range of the Earth and terrestrial planets is accessible to direct study. The latter makes the diamond cell especially suited for in situ analyses, allowing application of a growing range of material probes. The diamonds used in these experiments have flat outlet surfaces that range from 0.05 to 1 mm in diameter depending on the pressure range of interest. Owing to the small surface area over which force is applied, only modest loading forces are required to achieve high pressures.

The sample itself is contained within a small hole ($\sim 0.03 - 0.5 \mu\text{m}$) in a thin metal gasket between the anvils. The main disadvantage of the diamond cell involves the small volume of compressed sample. For stable operation, the metal gasket between the anvils is initially thin ($\sim 30 \mu\text{m}$) and plastic deformation with increasing load leads to further thinning such that at ~ 100 GPa, the sample thickness may be only a few micrometers. The resulting sample chamber volumes decrease from dimensions of 10^{-2}mm^3 at $P \sim 10$ GPa to 10^{-5}mm^3 at $P \sim 100$ GPa. Thus, there is a requirement for highly sensitive analytical techniques and this has led to a natural marriage between high-brilliance synchrotron sources and the diamond anvil cell.

Measurement of equilibrium thermodynamic properties at high pressures and temperatures requires that the experiments be conducted under hydrostatic stress conditions. The uniaxial load in a diamond anvil cell is transformed to a hydrostatic pressure by surrounding the sample with a fluid pressure medium. However, above 16 GPa; at room temperature, all known media freeze, resulting in development of some degree of non-hydrostatic stresses. In practice, samples are often surrounded by a solid pressure-transmitting medium, thereby generating a quasi-hydrostatic stress state. Rare gas solids (He, Ar, Ne) are often used for this purpose, but other soft materials (e.g. NaCl) are also employed. In addition, differential stresses can be relieved by annealing the sample at high temperature using the laser-heating technique discussed later.

Differential stresses can be often readily monitored and characterized by measuring either the relative variations of the lattice parameters or the ellipticity of diffraction rings together with lattice strain theory.

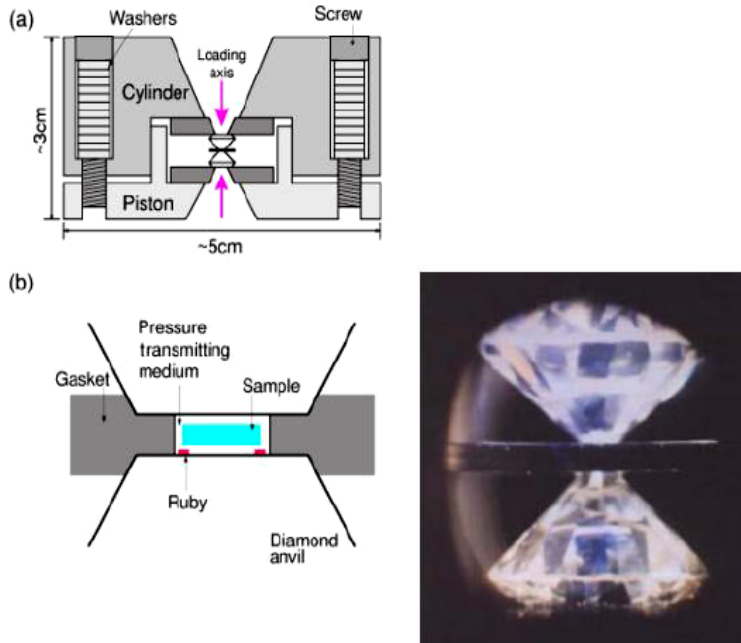


Figure 4: Schematic illustration of diamond anvil cell. (Right) Photomicrograph through a side opening in the cell showing diamond anvils and metal gasket between them. From figure 6 of Duffy 2005.

Pressure measurement in the diamond anvil cell relies on the use of calibration standards. One common method involves measurements of the R1 fluorescence wavelength of small ruby crystals placed in the sample chamber excited using visible laser irradiation. This ruby fluorescence scale has been calibrated against room temperature isotherms derived from shock Hugoniot data. The accuracy of the ruby scale has been verified to be within $\pm 1\%$ up to 55 GPa data, but its accuracy declines at higher pressures. The development of improved high $P - T$ pressure standards is an important area of research.

Diamond anvil cell technology has undergone continual refinement since its inception. The needs of synchrotron experiments have driven the development of symmetric and panoramic designs, as well as improvements to x-ray transparent gaskets and baking plates (for a recent review on diamond anvil cells see Basset, 2009).

Synchrotron techniques

The development and growth of dedicated beamlines for high pressure research at second and third generation synchrotron sources has enabled high pressure studies to exploit a number of desirable characteristics of synchrotron radiation. High x-ray energies are valuable because of their ability to penetrate the pressure confining medium. High intensities provide for rapid data accumulation on small weakly scattering samples. The small divergence of the beam enables achievement of small x-ray spots with slits or focusing optics that allow for higher intensities, isolate the pressure-confining medium and restrict the data collection to regions of minimal pressure and temperature gradients. The synchrotron developments have been coupled with developments in x-ray optics and detectors that allow detection of the subtle features often required to properly determine the unit cell and determine or refine the crystal structure. The tuneability of synchrotron sources and advances in high resolution optics has allowed for development and application of resonant scattering and spectroscopic techniques (for a recent review see Duffy, 2005). Powder x-ray diffraction has been the workhorse technique for synchrotron based high pressure studies. Over the past two decades, energy dispersive diffraction has been a widely used technique for synchrotron based studies of equation of state, high P-T phase transitions, texture development, strength and rheology determination and melting studies. The use of angle dispersive polycrystalline diffraction techniques at high pressures has increased in recent years. At present, most of the third generation synchrotron sources that are either in commissioning state or in the first years of operation, have at least one experimental station devoted to angle dispersive high pressure research. In this technique, a monochromatic x-ray beam is directed through the pressure apparatus and the rings of the diffracted intensities are recorded using an image plate (IP) or CCD

detector. CCD detectors have the advantage that readout time is minimal which can be especially important for laser-heating experiments in the DAC. However, IPs have large active areas, and superior resolution can be obtained. The main advantage of the angle dispersive method is markedly better angular resolution of diffracted peaks. Subtle phase transformations have been identified in several systems that could not be detected by energy dispersive methods. Also, with a CCD or an IP detector, integration of the whole powder ring means that reasonable intensities can be obtained. The powder pattern can then be subject to whole profile structure refinement using Rietveld method to obtain the information on the evolution of structure parameters with pressure.

Selected applications of synchrotron research to the core: iron phase diagram

The P – T conditions of the Earth's solid inner core (330–363 GPa, 4000–6000 K) still exceed those achievable by direct static experimental investigation, thus synchrotron studies of the crystal structure, melt properties, equation of state, thermodynamic properties and electronic and magnetic properties of iron and iron alloys over a range of P – T conditions play an integral role in understanding and interpreting geophysical data for planetary cores across the solar system.

At low pressures and temperatures, iron has four solid phases: α - and β -Fe, body centered (bcc) phases that are stable at low P and T and at high T just below the melting point, respectively: γ -Fe, a face centered cubic phase (fcc) stable at high temperatures and ϵ -Fe, a hexagonal close packed (hcp) phase stable at high pressures and low temperatures. At higher pressures, there have been some reports from diamond anvil cell experiments of the existence of additional phases, including a double hexagonal closed packed phase (dhcp) (Saxena et al. 1995, Yoo et al. 1996 and Dubrovinsky et al. 1998), and an orthorhombic phase (Andraut et al 1997 and 2000). However, other high pressure studies have not observed these phases (Funamori et al. 1996, Shen et al. 1998, Uchida et al. 2001, Kubo et al. 2003 and Ma et al. 2004).

It is plausible that these polymorphs are metastable and related to temperature or stress gradients in the diamond cell (Shen et al. 1998, Andraut et al. 2000 and Ma et al. 2004). This conclusion is supported by multi-anvil experiments, under more uniform temperature conditions, that reported no evidence for these phases at conditions up to

44 GPa and 2100 K (Funamori et al. and 1996 and 1996 and Kubo et al. 2003) (the phase diagram of iron is shown in figure 5). Such conflicting experimental results highlight the complexity and difficulty of, in principle simple, high-pressure experiments. The melting of iron remains controversial. Early studies were based on either visual observations of melt in the laser-heated diamond cells or on measurements of temperatures resulting from shock compression. However, these methods produced conflicting results. The figure below summarizes constraints on the melting curve of iron. Phase boundaries to 100 GPa are based on synchrotron x-ray diffraction results. These are consistent with the latest theoretical calculations and calculated shock temperatures obtained recently. This convergence of results suggests that a consensus in the melting curve of Fe may be developing.

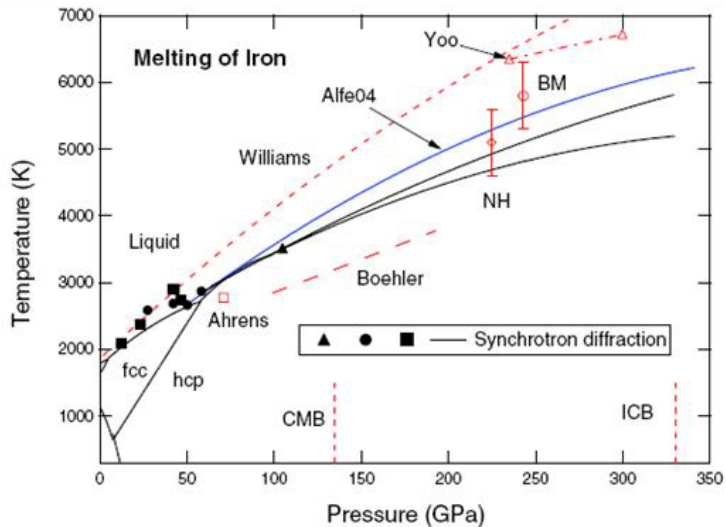


Figure 5: Phase diagram and melting curve of iron (the figure corresponds to figure 17 in Duffy (2005)). The solid black symbols are melt observations from synchrotron radiations experiments (Andraut et al, 2000, Ma et al. 2004 and Shen et al. 2004) and the solid black lines show phase boundaries and melting curve consistent with these results and extrapolated to higher pressures (Ma et al.2004). Other constraints on the melting line are from theory (AlFeO4) (Alfe et al. 2004), shock compression and static compression with visual observations (Williams et al. 1987 and Boehler 1993) fcc=face centred cubic phase (γ) and hcp (ϵ). ICB=inner core boundary and CMB=core-mantle boundary.

Extrapolation of the synchrotron-based melting curve yields melting temperatures for Fe at the inner core boundary of 5200 – 5900 K, whereas theoretical calculations yield a value near 6300 K.

Synchrotron light in challenging samples: small in size or in quantity

Deducing the mantle from the oxidation state of iron in ancient rock.

Ancient rocks yield information about conditions on and in the early Earth. New and more sophisticated techniques are being used to extract this information from precious pieces of the ancient Earth (“deducing the reducing mantle” as it was described in McDonough, 2008). Berry et al, 2008 reported the first results obtained by applying a new approach to estimating the oxidation-reduction (redox) condition of Earth's upper mantle during the Archaen era, some 2,700 million years ago. Their study is based on the ratio of different oxidized states of iron (Fe^{3+} to Fe^{2+}) in inclusions of ancient komatiite rock, trapped in crystals preserved in ancient lava flows in Zimbabwe (see figure 6). The crystals should have protected the inclusions from subsequent alteration, which should thus reflect the native lave state.

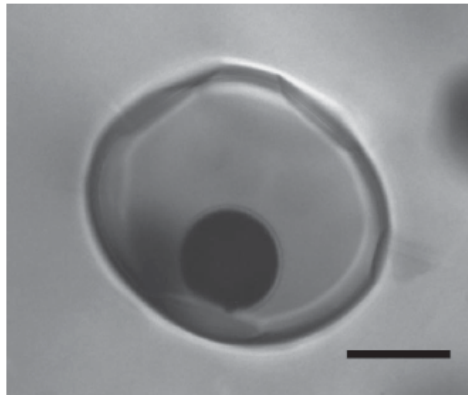


Figure 6: Optical image of an olivine-hosted melt inclusion (after heating) from a komatiite of the Belingwe belt, Zimbabwe. The inclusion comprises quenched melt (glass) and a dark 'shrinkage bubble'; scale bar, 20 μm . The figure corresponds to figure 3 of Berry et al. (2008)

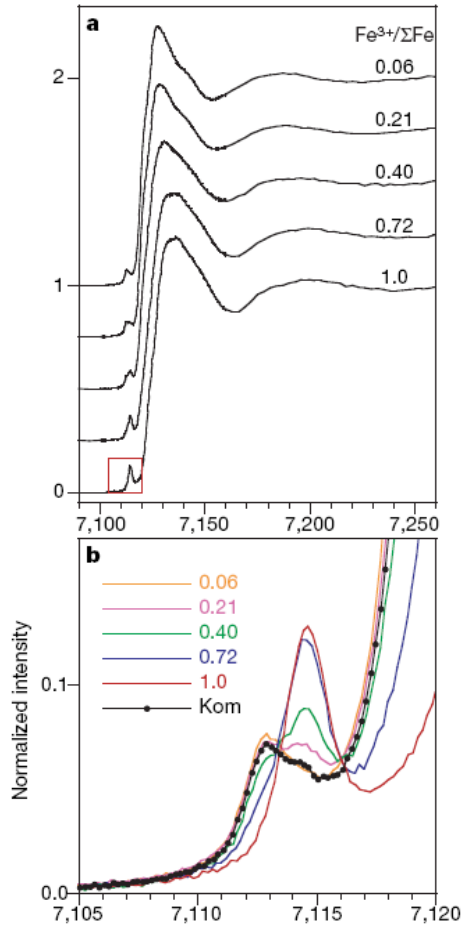


Figure 7: Iron K-edge spectra of quenched silicate melts a) Spectra of synthetic MORB glass standard with $Fe^{3+}/\Sigma Fe$ values indicated. Spectra have been shifted for clarity. b) XANES pre-edge region, indicated by a box in a) showing the $1s \rightarrow 3d$ transition of both the MORB standards and a natural komatiite mel inclusion (Kom). The figures correspond to figure 1a and b of McDonough 2008.

The authors accurately obtain $Fe^{3+}/\Sigma Fe$ from individual melt inclusions. $Fe^{3+}/\Sigma Fe$ in silicate glasses can be determined by redox titrations, commonly referred to as 'wet chemistry', and Mossbauer spectroscopy, but these methods lack spatial resolution and are generally restricted to bulk samples. Electron energy-loss spectroscopy and the

electron microprobe have the spatial resolution desired, but the techniques are unlikely to be suitable for the analysis of glass inclusions, owing to the high electron beam fluxes involved and the likelihood of beam-induced changes in oxidation state occurring. X-ray absorption near-edge structure (XANES) spectroscopy, which has micrometer spatial resolution, is non-destructive, element specific and requires no sample preparation other than a polished surface, has promised much for a number of years, but accurate quantification of $\text{Fe}^{3+}/\Sigma\text{Fe}$ has been hindered by the need for compositionally matched standards and a lack of sufficient precision in the limited $\text{Fe}^{3+}/\Sigma\text{Fe}$ range of most terrestrial samples.

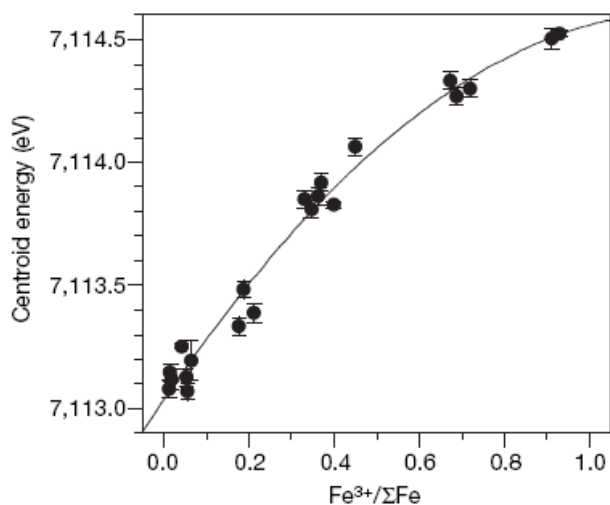


Figure 8: Calibration curve for determining $\text{Fe}^{3+}/\Sigma\text{Fe}$ from XANES pre-edge centroid energy. The figure corresponds to figure 2 of Berry et al. (2003).

However, it has been shown recently that oxidation state ratios in glasses can be determined with great accuracy and precision, by preparing a series of standards as a function of oxygen fugacity (Berry et al. 2003 and Berry 2004). The authors proved that the accurate and precise calculation of the $\text{Fe}^{3+}/\Sigma\text{Fe}$ can be achieved by selecting standards that contain iron at similar sites as the material of study and that all spectra is processed identically.

Berry et al. chose as glass standards mid-ocean-ridge basalt (MORB), tholeiite, pantellerite and andesite compositions and proved the validity of the method by determining the $\text{Fe}^{3+}/\Sigma\text{Fe}$ for a number of olivine-hosted MORB melt inclusions (the obtained values are in agreement with the literature Bezos and Humler, 2005). The Fe K absorption edge comprises features that have been simplified as transitions to bound states: $1s \rightarrow 3d$ (pre-edge), $1s \rightarrow 4s$ (shoulder) and $1s \rightarrow 4p$ (edge crest) (Shulman et al. 1976 and Waychumas et al. 1983). The established method for determining the $\text{Fe}^{3+}/\Sigma\text{Fe}$ ratio is the energy of the $1s \rightarrow 3d$ pre-edge transition. This feature shifts to higher energy with increasing $\text{Fe}^{3+}/\Sigma\text{Fe}$ (Bajt et al. 1994), allowing for an empirical calibration curve to be constructed.

The methodology was then applied to determining the $\text{Fe}^{3+}/\Sigma\text{Fe}$ ratio of komatiite melt inclusions. XANES spectra of the MORB standards is shown in figure 7a (with the $\text{Fe}^{3+}/\Sigma\text{Fe}$ indicated). The pre-edge region of the XANES spectrum of komatiite melt is shown in figure 7b, as well as the spectra of the calibration standards. Using the calibration curve (Figure 8), the average value of $\text{Fe}^{3+}/\Sigma\text{Fe}$ of four komatiite inclusions the results are consistent with anomalously hot mantle model for the formation of the komatiite. The energy resolution shown in figure 8 is achieved by the high resolution Si111 monochromator installed in beamline 13-ID-C, GeoSoilEnviroCARS (GSECARS, University of Chicago), of the Advanced Photon Source (Argonne National Laboratory, USA). More work is needed if we are to find and analyze melt inclusions from other komatiites and ancient lavas, with the aim of building a comparative perspective on the secular evolution of the oxidation state of lavas from various tectonic settings. The analytical methodology applied by Berry et al. is now available for studying minute geological time-capsules, and so opens the door for many other studies. There are plenty of old hypotheses to be tested with this new tool.

The origins of carbonado diamonds

“Carbonado” or “black diamonds” are unlike gem diamonds sourced singly in kimberlite or lamproite pipes, sites of explosive eruptivity stemming from deep in the

Earth's mantle. Such black diamonds are polycrystalline, being formed of minute crystals clumped together – this gives them their dark appearance. The polycrystalline aggregates are typically of irregular shape and characteristically they exhibit greyblack surfaces that resemble those of coal and have exceptionally high porosities. Nevertheless, their carbon atoms have the arrangement of diamond, and there is no question that they are form of diamond. They are reported not to occur associated with pipes, but only in placers, in single layer sediments. The possible origin of carbonado is still controversial. A recent review entitled “the carbonado diamond cunumdrum” (McCall 2009) was triggered by a short note by Hansen (2007) in *Geotimes* (Hansen 2007), based on the publication by Garai et al (2006). Garai and coworkers propose the extraterrestrial origin of carbonado diamond, for that they used the infra-red FTIR absorption spectra of Brazilian and CAR (from Central African Republic) carbonados to detect single nitrogen impurities and hydrogen. The authors believe that the diamonds were formed in a hydrogen rich interstellar space environment, ant that they come from a fragmented body of asteroidal proportions.

Their argument is based on “overwhelming evidence of similarity to presolar diamonds in meteorites and interstellar diamonds”. And according to McCall, the author of the review (McCall 2009), “the experimental results are convincing; yet they are only concerned about the experimental results, and they make no attempt to explain how the carbonados were aggregated into polycrystalline masses, nor does it explain their concentration in conglomerates/placers”. In summary there is still much work to do to solve the diamond black conumdrum. However, Garai et al, proved that by using a synchrotron radiation source with a 100 times better signal-to-noise ratio than the laboratory instrument they obtained the first complete FTIR absorption spectra of carbonado diamond. Figure 9 shows a representative CAR carbonado IR absorption spectrum obtained with a “laboratory source” (IR microprobe) and the one obtained in a synchrotron source (beamline U2b beamline at the National Synchrotron Light Source (NSLS) at Brookhaven National Laboratory, it should be noted that NSLS is a 2nd generation synchrotron source). The figure shows that both data sets have similar features, and that the synchrotron data present better resolution and statistics. This is more clear in the frequency range, 1000 – 1300 cm⁻¹ (assigned as substitutional N in

diamond samples) as well as in the $3000 - 2800 \text{ cm}^{-1}$ region (assigned as C-H stretching bands). The three peaks indicated by arrows in the C-H stretching region (top curve) are not resolved with the laboratory source. The same occurs with the peaks at 974 and 904 cm^{-1} . Present IR beamlines at modern synchrotrons make use of the intense edge bending magnet radiation which allows, with suitable optics, to perform 2D images with micrometer resolution of selected absorption bands.

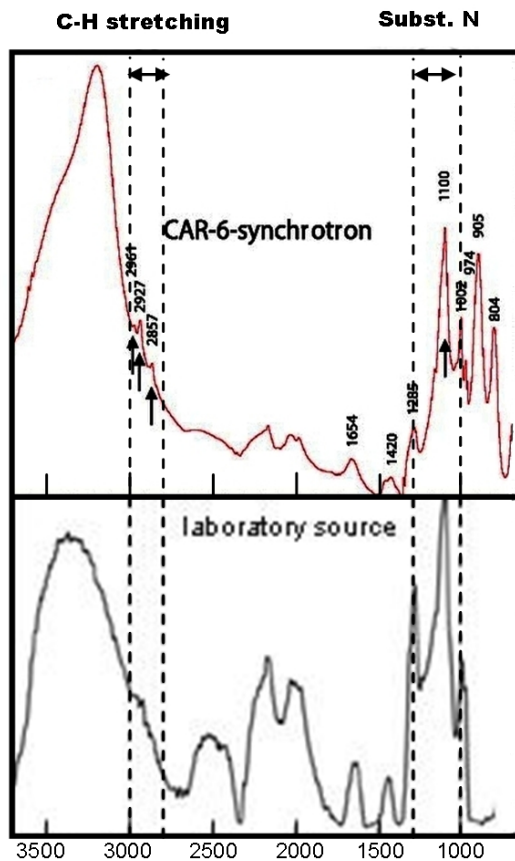


Figure 9: Bottom, Representative IR absorption spectra of CAR carbonado (the figure corresponds to figure 5 of Kagi et al, 2008 (Kagi and Fokura, 2008)). Top, IR absorption spectra of CAR carbonado acquired at a synchrotron source. The C-H stretching bands and the band associated to Nitrogen impurities in diamond are marked for clarity. The figure corresponds to figure 2 of Garai et al, 2006. The x-axis dimensions are in cm^{-1}

Conclusions

The diffraction based techniques and spectroscopies that will be available at Alba will offer a new scenario for analyzing specimens of geological interest. We have only shown a few selected examples but the domains of application of synchrotron techniques comprise soil analysis and contamination, air pollutants (ash, microparticules), nuclear waste disposal and other applications to environmental sciences.

References

- Ahrens, T J, Holland, K G and Chen, G Q (2002). *Geophys. Res. Lett.* 29 1150.
- Alfe, D, Vocadlo L, Price, G D and Gillan, M J (2004) *J. Phys.: Condens. Matter* 16 S973–S982.
- Andraut, D, Fiquet G, Charpin T and le Bihan T (2000) *Am. Mineral.* 85 364–71.
- Andraut, D., Fiquet, G., Kunz, M., Visocekas, F. and Hausermann, D. (1997) *Science* 278 831–4.
- Bajt, S., Sutton, S. R. and Delaney, J. S. (1994) *Geochimica et Cosmochimica Acta*, 58, 5209–5214.
- Bassett, W. A. (2009) *High Pressure Research* 29 CP5-186.
- Berry, A. J. and O’Neill, H. St. C. (2004) *Am. Mineral.* 89 790–798.
- Berry, A. J., Danyushevsky, L. V., O’Neill, H. St. C., Newvillem M. and Sutton S R 2008 *Nature* 455 960-3.
- Berry, A. J, O’Neill, H. St. C., Jayasuriya, K. D., Campbell, S. J. and Foran, G. J. (2003) *Am. Mineral.* 88 967–977.
- Bezos, A. and Humler, E. (2005) *Geochim. Cosmochim. Acta* 69, 711–725.
- Boehler, R. (1993) *Nature* 363 534-6.
- Bordas, et al. *Proceed. EPAC* (2004) , Lucerne, Switzerland pg. 2326.
- Brown, J. M. and McQueen, R. G. (1996) *J. Geophys. Res.* 91 7485–94.
- Dubrovinsky, L. S., Saxena, S. K. and Lazor P. (1998) *Eur. J. Mineral.* 10 43–7.
- Duffy, T. S. (2005) *Rep. Prog. Phys.* 68 1811-1859.
- Funamori N., Yagi T. and Uchida T. (1996) *Geophys. Res. Lett.* 23 953–6.
- Garai, J. and Haggerty, S. E. (2006) *The Astrophysical Journal*, 653 L153–L156.

- Hansen, K (2007) *Geotimes* 52 15-16.
- Hazen, R. M. and Downs, R. T. (editors). (2000) *Reviews in mineralogy and Geochemistry, Volume 41. High-Temperature and High-Pressure Crystal Chemistry*. Mineralogical Society of America,.
- Kagi, H and Fukura, S (2008) *Eur. J. Mineral.* 20 387-393.
- Kubo, A., Ito, E., Katsura, T., Shinmei, T., Yamada, H., Nishikawa, O., Song, M. S. and Funakoshi, K. (2003) *Geophys. Res. Lett.* 30 1126.
- Ma, Y. Z., Somayazulu, M., Shen, G. Y., Mao, H. K., Shu, J. F. and Hemley, R. J. (2004) *Phys. Earth Planet. Int.* 143–144.
- McCall, G. J. H. (2009) *Earth-Science Reviews* 93 85-91.
- McDonough, W. F. (2008) *Nature* 455 881-3.
- Munoz, et al. Proc. of (2005) Particle Accelerator Conference, Knoxville, Tennessee, pp 3777.
- Nguyen, J. H. and Holmes N. C. (2004) *Nature* 427 339–42.
- Saxena, S. K., Dubrovinsky, L. S., Haggkvist, P., Cerenius, Y., Shen, G. and Mao, H. K. (1995) *Science* 269, 1703–4.
- Shen, G. Y., Prakapenka, V. B., Rivers M. L. and Sutton S. R. (2004) *Phys. Rev. Lett.* 92 185701.
- Shen G., Mao, H.-K., Hemley, R. J., Duffy, T. S. and Rivers, M. L. (1998) *Geophys. Res. Lett.* 25 373–6.
- Shulman, R. G., Yafet, Y., Eisenberger, P., and Blumberg, W. E. (1976) *Proceedings of the National Academy of Science*, 73, 1384–1388.
- Uchida T., Wang, Y. B., Rivers, M. L. and Sutton, S. R. (2001) *J. Geophys. Res.* 106 21799–810
- Waychunas, G.A., Apter, M.J., and Brown Jr., G.E. (1983) *Physics and Chemistry of Minerals* 10 1–9.
- Williams, Q., Jeanloz, R., Bass, J., Svendsen, B. and Ahrens, T. J. (1987) *Science* 236 181–2.
- Yoo, C. S., Holmes, N. C., Ross, M., Webb, D. J. and Pike, C. (1993) *Phys. Rev. Lett.* 70 3931–4.

Yoo, C. S., Soderlind, P., Moriarty, J. A. and Cambell, A. J. (1996) Phys. Lett. A 214 65–70.